



KEK preprint 2001-3

Belle preprint 2001-2

# A Measurement of the Branching Fraction for the Inclusive $B \rightarrow X_s \gamma$ Decays with Belle

The Belle Collaboration

K. Abe<sup>10</sup>, K. Abe<sup>37</sup>, I. Adachi<sup>10</sup>, Byoung Sup Ahn<sup>15</sup>, H. Aihara<sup>38</sup>,  
 M. Akatsu<sup>20</sup>, G. Alimonti<sup>9</sup>, K. Aoki<sup>10</sup>, K. Asai<sup>21</sup>, Y. Asano<sup>43</sup>, T. Aso<sup>42</sup>,  
 V. Aulchenko<sup>2</sup>, T. Aushev<sup>13</sup>, A. M. Bakich<sup>34</sup>, E. Banas<sup>16</sup>, W. Bartel<sup>10,6</sup>,  
 S. Behari<sup>10</sup>, P. K. Behera<sup>44</sup>, D. Beilene<sup>2</sup>, A. Bondar<sup>2</sup>, A. Bozek<sup>16</sup>,  
 T. E. Browder<sup>9</sup>, B. C. K. Casey<sup>9</sup>, P. Chang<sup>24</sup>, Y. Chao<sup>24</sup>, B. G. Cheon<sup>33</sup>,  
 S.-K. Choi<sup>8</sup>, Y. Choi<sup>33</sup>, Y. Doi<sup>10</sup>, J. Dragic<sup>18</sup>, A. Drutskoy<sup>13</sup>, S. Eidelman<sup>2</sup>,  
 Y. Enari<sup>20</sup>, R. Enomoto<sup>10,11</sup>, F. Fang<sup>9</sup>, H. Fujii<sup>10</sup>, C. Fukunaga<sup>40</sup>,  
 M. Fukushima<sup>11</sup>, A. Garmash<sup>2,10</sup>, A. Gordon<sup>18</sup>, K. Gotow<sup>45</sup>, H. Guler<sup>9</sup>,  
 R. Guo<sup>22</sup>, J. Haba<sup>10</sup>, H. Hamasaki<sup>10</sup>, K. Hanagaki<sup>30</sup>, F. Handa<sup>37</sup>, K. Hara<sup>28</sup>,  
 T. Hara<sup>28</sup>, T. Haruyama<sup>10</sup>, N. C. Hastings<sup>18</sup>, K. Hayashi<sup>10</sup>, H. Hayashii<sup>21</sup>,  
 M. Hazumi<sup>28</sup>, E. M. Heenan<sup>18</sup>, Y. Higasino<sup>20</sup>, I. Higuchi<sup>37</sup>, T. Higuchi<sup>38</sup>,  
 H. Hirano<sup>41</sup>, T. Hojo<sup>28</sup>, Y. Hoshi<sup>36</sup>, W.-S. Hou<sup>24</sup>, S.-C. Hsu<sup>24</sup>, H.-C. Huang<sup>24</sup>,  
 S. Ichizawa<sup>39</sup>, Y. Igarashi<sup>10</sup>, T. Iijima<sup>10</sup>, H. Ikeda<sup>10</sup>, K. Ikeda<sup>21</sup>, K. Inami<sup>20</sup>,  
 A. Ishikawa<sup>20</sup>, H. Ishino<sup>39</sup>, R. Itoh<sup>10</sup>, G. Iwai<sup>26</sup>, H. Iwasaki<sup>10</sup>, Y. Iwasaki<sup>10</sup>,  
 D. J. Jackson<sup>28</sup>, P. Jalocha<sup>16</sup>, H. K. Jang<sup>32</sup>, M. Jones<sup>9</sup>, R. Kagan<sup>13</sup>,  
 H. Kakuno<sup>39</sup>, J. Kaneko<sup>39</sup>, J. H. Kang<sup>46</sup>, J. S. Kang<sup>15</sup>, P. Kapusta<sup>16</sup>,  
 N. Katayama<sup>10</sup>, H. Kawai<sup>3</sup>, N. Kawamura<sup>1</sup>, T. Kawasaki<sup>26</sup>, H. Kichimi<sup>10</sup>,  
 D. W. Kim<sup>33</sup>, Heejong Kim<sup>46</sup>, H. J. Kim<sup>46</sup>, Hyunwoo Kim<sup>15</sup>, S. K. Kim<sup>32</sup>,  
 K. Kinoshita<sup>5</sup>, K. Korotushenko<sup>30</sup>, P. Krokovny<sup>2</sup>, R. Kulasiri<sup>5</sup>, S. Kumar<sup>29</sup>,  
 T. Kuniya<sup>31</sup>, E. Kurihara<sup>3</sup>, A. Kuzmin<sup>2</sup>, Y.-J. Kwon<sup>46</sup>, J. S. Lange<sup>7</sup>,  
 M. H. Lee<sup>10</sup>, S. H. Lee<sup>32</sup>, H.B. Li<sup>12</sup>, D. Liventsev<sup>13</sup>, R.-S. Lu<sup>24</sup>, A. Manabe<sup>10</sup>,  
 T. Matsubara<sup>38</sup>, S. Matsui<sup>20</sup>, S. Matsumoto<sup>4</sup>, T. Matsumoto<sup>20</sup>, Y. Mikami<sup>37</sup>,

K. Misono<sup>20</sup>, K. Miyabayashi<sup>21</sup>, H. Miyake<sup>28</sup>, H. Miyata<sup>26</sup>, L. C. Moffitt<sup>18</sup>,  
 G. R. Moloney<sup>18</sup>, G. F. Moorhead<sup>18</sup>, S. Mori<sup>43</sup>, A. Murakami<sup>31</sup>,  
 T. Nagamine<sup>37</sup>, Y. Nagasaka<sup>19</sup>, Y. Nagashima<sup>28</sup>, T. Nakadaira<sup>38</sup>,  
 E. Nakano<sup>27</sup>, M. Nakao<sup>10</sup>, J. W. Nam<sup>33</sup>, S. Narita<sup>37</sup>, Z. Natkaniec<sup>16</sup>,  
 K. Neichi<sup>36</sup>, S. Nishida<sup>17</sup>, O. Nitoh<sup>41</sup>, S. Noguchi<sup>21</sup>, T. Nozaki<sup>10</sup>, S. Ogawa<sup>35</sup>,  
 T. Ohshima<sup>20</sup>, Y. Ohshima<sup>39</sup>, T. Okabe<sup>20</sup>, T. Okazaki<sup>21</sup>, S. Okuno<sup>14</sup>,  
 S. L. Olsen<sup>9</sup>, W. Ostrowicz<sup>16</sup>, H. Ozaki<sup>10</sup>, H. Palka<sup>16</sup>, C. S. Park<sup>32</sup>,  
 C. W. Park<sup>15</sup>, H. Park<sup>15</sup>, L. S. Peak<sup>34</sup>, M. Peters<sup>9</sup>, L. E. Piilonen<sup>45</sup>,  
 E. Prebys<sup>30</sup>, J. L. Rodriguez<sup>9</sup>, N. Root<sup>2</sup>, M. Rozanska<sup>16</sup>, K. Rybicki<sup>16</sup>,  
 J. Ryuko<sup>28</sup>, H. Sagawa<sup>10</sup>, Y. Sakai<sup>10</sup>, H. Sakamoto<sup>17</sup>, M. Satapathy<sup>44</sup>,  
 A. Satpathy<sup>10,5</sup>, S. Schrenk<sup>45,5</sup>, S. Semenov<sup>13</sup>, K. Senyo<sup>20</sup>, M. E. Sevior<sup>18</sup>,  
 H. Shibuya<sup>35</sup>, B. Shwartz<sup>2</sup>, V. Sidorov<sup>2</sup>, J.B. Singh<sup>29</sup>, S. Stanić<sup>43</sup>, A. Sugi<sup>20</sup>,  
 A. Sugiyama<sup>20</sup>, K. Sumisawa<sup>28</sup>, T. Sumiyoshi<sup>10</sup>, K. Suzuki<sup>3</sup>, S. Suzuki<sup>20</sup>,  
 S. Y. Suzuki<sup>10</sup>, S. K. Swain<sup>9</sup>, H. Tajima<sup>38</sup>, T. Takahashi<sup>27</sup>, F. Takasaki<sup>10</sup>,  
 M. Takita<sup>28</sup>, K. Tamai<sup>10</sup>, N. Tamura<sup>26</sup>, J. Tanaka<sup>38</sup>, M. Tanaka<sup>10</sup>,  
 Y. Tanaka<sup>19</sup>, G. N. Taylor<sup>18</sup>, Y. Teramoto<sup>27</sup>, M. Tomoto<sup>20</sup>, T. Tomura<sup>38</sup>,  
 S. N. Tovey<sup>18</sup>, K. Trabelsi<sup>9</sup>, T. Tsuboyama<sup>10</sup>, Y. Tsujita<sup>43</sup>, T. Tsukamoto<sup>10</sup>,  
 S. Uehara<sup>10</sup>, K. Ueno<sup>24</sup>, N. Ujiie<sup>10</sup>, Y. Unno<sup>3</sup>, S. Uno<sup>10</sup>, Y. Ushiroda<sup>17</sup>,  
 Y. Usov<sup>2</sup>, S. E. Vahsen<sup>30</sup>, G. Varner<sup>9</sup>, K. E. Varvell<sup>34</sup>, C. C. Wang<sup>24</sup>,  
 C. H. Wang<sup>23</sup>, M.-Z. Wang<sup>24</sup>, T.J. Wang<sup>12,†</sup>, Y. Watanabe<sup>39</sup>, E. Won<sup>32</sup>,  
 B. D. Yabsley<sup>10</sup>, Y. Yamada<sup>10</sup>, M. Yamaga<sup>37</sup>, A. Yamaguchi<sup>37</sup>,  
 H. Yamamoto<sup>9</sup>, H. Yamaoka<sup>10</sup>, Y. Yamaoka<sup>10</sup>, Y. Yamashita<sup>25</sup>,  
 M. Yamauchi<sup>10</sup>, S. Yanaka<sup>39</sup>, M. Yokoyama<sup>38</sup>, K. Yoshida<sup>20</sup>, Y. Yusa<sup>37</sup>,  
 H. Yuta<sup>1</sup>, C.C. Zhang<sup>12</sup>, J. Zhang<sup>43</sup>, Y. Zheng<sup>9</sup>, V. Zhilich<sup>2</sup>, and D. Žontar<sup>43</sup>

<sup>1</sup>*Aomori University, Aomori*

<sup>2</sup>*Budker Institute of Nuclear Physics, Novosibirsk*

<sup>3</sup>*Chiba University, Chiba*

<sup>4</sup>*Chuo University, Tokyo*

<sup>5</sup>*University of Cincinnati, Cincinnati, OH*

<sup>6</sup>*Deutsches Elektronen-Synchrotron, Hamburg*

<sup>7</sup>*University of Frankfurt, Frankfurt*

<sup>8</sup>*Gyeongsang National University, Chinju*

<sup>9</sup>*University of Hawaii, Honolulu HI*

<sup>10</sup>*High Energy Accelerator Research Organization (KEK), Tsukuba*

<sup>11</sup>*Institute for Cosmic Ray Research, University of Tokyo, Tokyo*

<sup>12</sup>*Institute of High Energy Physics, Chinese Academy of Sciences, Beijing*

<sup>13</sup>*Institute for Theoretical and Experimental Physics, Moscow*

<sup>14</sup>*Kanagawa University, Yokohama*

<sup>15</sup>*Korea University, Seoul*

<sup>16</sup>*H. Niewodniczanski Institute of Nuclear Physics, Krakow*  
<sup>17</sup>*Kyoto University, Kyoto*  
<sup>18</sup>*University of Melbourne, Victoria*  
<sup>19</sup>*Nagasaki Institute of Applied Science, Nagasaki*  
<sup>20</sup>*Nagoya University, Nagoya*  
<sup>21</sup>*Nara Women's University, Nara*  
<sup>22</sup>*National Kaohsiung Normal University, Kaohsiung*  
<sup>23</sup>*National Lien-Ho Institute of Technology, Miao Li*  
<sup>24</sup>*National Taiwan University, Taipei*  
<sup>25</sup>*Nihon Dental College, Niigata*  
<sup>26</sup>*Niigata University, Niigata*  
<sup>27</sup>*Osaka City University, Osaka*  
<sup>28</sup>*Osaka University, Osaka*  
<sup>29</sup>*Panjab University, Chandigarh*  
<sup>30</sup>*Princeton University, Princeton NJ*  
<sup>31</sup>*Saga University, Saga*  
<sup>32</sup>*Seoul National University, Seoul*  
<sup>33</sup>*Sungkyunkwan University, Suwon*  
<sup>34</sup>*University of Sydney, Sydney NSW*  
<sup>35</sup>*Toho University, Funabashi*  
<sup>36</sup>*Tohoku Gakuin University, Tagajo*  
<sup>37</sup>*Tohoku University, Sendai*  
<sup>38</sup>*University of Tokyo, Tokyo*  
<sup>39</sup>*Tokyo Institute of Technology, Tokyo*  
<sup>40</sup>*Tokyo Metropolitan University, Tokyo*  
<sup>41</sup>*Tokyo University of Agriculture and Technology, Tokyo*  
<sup>42</sup>*Toyama National College of Maritime Technology, Toyama*  
<sup>43</sup>*University of Tsukuba, Tsukuba*  
<sup>44</sup>*Utkal University, Bhubaneswar*  
<sup>45</sup>*Virginia Polytechnic Institute and State University, Blacksburg VA*  
<sup>46</sup>*Yonsei University, Seoul*  
<sup>†</sup>*(deceased)*

---

## Abstract

We have measured the branching fraction of the inclusive radiative  $B$  meson decay  $B \rightarrow X_s \gamma$  to be

$$Br(B \rightarrow X_s \gamma) = (3.36 \pm 0.53(\text{stat}) \pm 0.42(\text{sys})^{+0.50}_{-0.54}(\text{th})) \times 10^{-4}.$$

The result is based on a sample of  $6.07 \times 10^6$   $B\bar{B}$  events collected at the  $\Upsilon(4S)$  resonance with the Belle detector at the KEKB asymmetric  $e^+e^-$  storage ring.

*PACS:* 13.40.Hq, 14.40.Nd, 14.65.Fy

---

In the framework of the Standard Model (SM), the inclusive decay  $B \rightarrow X_s \gamma$ , where  $X_s$  is a hadronic recoil system containing an  $s$  quark, proceeds primarily through the electroweak penguin diagrams of the radiative  $b \rightarrow s \gamma$  transition. These diagrams are of interest because they have loops where non-SM particles, such as charged Higgs bosons or SUSY particles, can contribute and potentially produce deviations from SM expectations. An SM branching fraction calculation for  $B \rightarrow X_s \gamma$  that includes next-to-leading order QCD corrections has an expected precision of 10% [1]. Experimental measurements of the branching fraction at this level of precision are useful for identifying or limiting non-SM theories [2].

The signature for this decay is a high energy photon accompanied by a kaon. The monochromatic photon energy from the two-body decay  $b \rightarrow s \gamma$  is smeared by gluon emission, the Fermi motion of the  $b$  quark inside the  $B$  meson, and the  $B$  meson momentum in the  $\Upsilon(4S)$  center-of-mass (CM) frame. A semi-inclusive analysis is used to reconstruct the  $B \rightarrow X_s \gamma$  decay from a primary photon, a kaon and multiple pions.

The  $B \rightarrow X_s \gamma$  decay is studied with the Belle detector at the KEKB asymmetric  $e^+e^-$  storage ring [3]. The dataset consists of a sample of  $6.07 \times 10^6$   $B\bar{B}$  events corresponding to an integrated luminosity of  $5.8 \text{ fb}^{-1}$  taken at the  $\Upsilon(4S)$  resonance ( $\sqrt{s} = 10.58 \text{ GeV}$ ), and an off-resonance background sample of  $0.6 \text{ fb}^{-1}$  taken 60 MeV below  $\Upsilon(4S)$ . The beam energies at the  $\Upsilon(4S)$  resonance are 3.5 GeV for positrons and 8.0 GeV for electrons. Quantities used in this analysis are defined in the CM frame, in which the beam energy  $E_{beam}$  is defined as  $\sqrt{s}/2$ . Inclusion of charge conjugated modes are implied throughout the text.

A full description of the Belle detector is given in ref. [4]; here we briefly describe the components relevant for this analysis. Charged tracks are reconstructed inside a 1.5 T super-conducting solenoid magnet with a 50 layer central drift chamber (CDC), that covers the laboratory polar angle  $17^\circ < \theta_{lab} < 150^\circ$ . Tracks are fitted through the CDC and a three layer double sided silicon vertex detector (SVD), with a transverse momentum resolution of  $(\sigma_{p_t}/p_t)^2 = (0.0019p_t)^2 + (0.0034)^2$  ( $p_t$  in  $\text{GeV}/c$ ). For particle identification, we combine information from three detectors. The high momentum range, typically from 1 to 3.5  $\text{GeV}/c$ , is covered by a silica aerogel Cherenkov counter (ACC) system, providing threshold-type kaon-to-pion separation. The momentum range below 1.5  $\text{GeV}/c$  is covered by a time-of-flight (TOF) counter system, and the very low and high momentum ranges are accessible with  $dE/dx$  information from the CDC. Photons are detected by an electromagnetic calorimeter (ECL) located between the particle identification devices and the solenoid coil. The entire tracking acceptance is covered with 8736 CsI(Tl) crystals that are typically  $5.5 \times 5.5 \text{ cm}^2$  in cross-section at the front surface and  $16.2 X_0$  in depth. The photon energy resolution is  $(\sigma_E/E)^2 =$

$0.013^2 + (0.0007/E)^2 + (0.008/E^{1/4})^2$  ( $E$  in GeV), which is better than 2% for the primary photons used in this analysis. The Belle detector is modelled with the GEANT program [5] to simulate the detector response. Both the data and the Monte Carlo (MC) events [6] are reconstructed with the same program.

Hadronic events are selected with an efficiency of 99% for  $B\bar{B}$  final states. Events with at least three tracks from the interaction region and  $> 0.2\sqrt{s}$  visible energy are selected. The QED and  $\tau^+\tau^-$  events that remain are removed using ECL information and event topology.

Photon candidates are selected from ECL clusters of  $5 \times 5$  crystals. Each photon candidate is required to have a laboratory energy greater than 20 MeV with no associated charged track, and shower shape consistent with an electromagnetic shower. We accept events in which the most energetic photon is in the barrel region ( $33^\circ < \theta_{lab} < 132^\circ$ ). We require 95% of its energy is concentrated in the central  $3 \times 3$  crystals. The efficiency of these criteria for the primary photon is 80%. In order to reject  $\pi^0$  and  $\eta$  mesons, we combine this primary photon candidate with any other photon (for  $\eta$  we only use photons with  $E_\gamma > 200$  MeV) and reject the event if the invariant mass of the two photons is within  $\pm 18$  MeV/ $c^2$  of  $M_{\pi^0}$  or  $\pm 32$  MeV/ $c^2$  of  $M_\eta$ .

Charged kaon candidates are selected using a kaon-to-pion likelihood ratio. For every charged track, likelihoods from ACC, TOF and  $dE/dx$  are calculated for pion and kaon hypotheses. A combined likelihood is constructed for each hypothesis, and a tight cut is applied on the likelihood ratio. Kaons are identified with a typical efficiency of 65% with 2% pion fake rate. All charged tracks that are not identified as kaons are considered to be pions.

The  $K_S^0 \rightarrow \pi^+\pi^-$  candidates are reconstructed from two oppositely charged tracks. The  $K_S^0$  momentum is recalculated with a vertex constrained fit. The candidates are then required to have an invariant mass within  $\pm 8$  MeV/ $c^2$  of  $M_{K^0}$  and a vertex that is displaced from the interaction point in a direction consistent with the  $K_S^0$  momentum. The  $K_S^0$  reconstruction efficiency is 65%. The  $\pi^0 \rightarrow \gamma\gamma$  candidates are reconstructed from two photons that have an invariant mass within  $\pm 16$  MeV/ $c^2$  of  $M_{\pi^0}$ . Then, the  $\pi^0$  momentum is recalculated with a mass constrained fit. The  $\pi^0$  reconstruction efficiency is 60%.

We reconstruct the recoil system  $X_s$  in 16 different final states of one charged kaon or  $K_S^0$  plus one to four pions which may include one  $\pi^0$ . We combine the primary photon with every  $X_s$  combination and calculate the opening angle  $\theta_{X_s\gamma}$  between  $\vec{p}_\gamma$  and  $\vec{p}_{X_s}$ , the energy difference  $\Delta E = E_\gamma + E_{X_s} - E_{beam}$  and the beam constrained mass  $M_{bc} = \sqrt{E_{beam}^2 - |\vec{p}_\gamma + \vec{p}_{X_s}|^2}$ . Then, we require  $\theta_{X_s\gamma} > 167^\circ$ ,  $M_{bc} > 5.2$  GeV/ $c^2$  and  $-0.15 < \Delta E/\text{GeV} < 0.1$ .

When multiple candidates are found in an event, the best candidate is selected as follows: If there is at least one charged kaon or pion that forms the  $X_s$  vertex with the run dependent beam profile constraint, the candidate with the largest vertex confidence level is chosen. The candidate with the largest  $\theta_{X_s\gamma}$  is chosen in the following cases: (1) there is no charged kaon or pion to form the vertex; (2) there remains an ambiguity whether to add a  $\pi^0$ ; or (3) there are several  $\pi^0$  and  $K_S^0$  candidates to choose from. After selecting the best candidate, we require  $M_{X_s} < 2.05 \text{ GeV}/c^2$ .

The largest background source is from continuum  $q\bar{q}$  production where the photon originates from initial state radiation or from high momentum neutral hadron decays such as  $\pi^0 \rightarrow \gamma\gamma$  with one undetected photon. In order to reduce and estimate the contribution of the  $q\bar{q}$  background, we introduce a new variable that exploits the topological difference between the jet-like  $q\bar{q}$  events and the spherical  $B\bar{B}$  events. We define the following variables in the  $B$  meson rest frame,

$$R_l = \frac{\sum_i |p_i||p_\gamma|P_l(\cos\theta_{i\gamma})}{\sum_i |p_i||p_\gamma|}, \quad r_l = \frac{\sum_{i,j} |p_i||p_j|P_l(\cos\theta_{ij})}{\sum_{i,j} |p_i||p_j|},$$

where  $P_l$  is a Legendre polynomial of order  $l$ , and  $i, j$  run over all the photons and charged tracks that are not used to form the  $B$  candidate. Then, we combine six of them into a Fisher discriminant

$$F = \sum_{l=2,4} \alpha_l R_l + \sum_{l=1,2,3,4} \beta_l r_l,$$

where the six coefficients  $\alpha_l$  and  $\beta_l$  are optimized to maximize the discrimination between signal and background as shown in Fig. 1. We call  $F$  the *Super Fox-Wolfram* (SFW) variable, since the terms are combined in such a way as to enhance the discriminating power of the original Fox-Wolfram moments [7]. We select events with  $F > 0.1$ , which is a compromise between the statistical significance of the signal and the size of the systematic error due to background subtraction. In order to estimate the  $q\bar{q}$  background contribution, we use the SFW sideband region of  $F < -1.5$ , where the signal fraction is only 0.7%.

In addition to the  $q\bar{q}$  background, there is a contribution from  $b \rightarrow c$  decays, in which  $B \rightarrow D^{(*)}\rho$  modes are dominant. This background, which does not contribute to the SFW sideband, is estimated by MC to be  $9.1 \pm 1.8$  events and is subtracted from the data sample.

The signal yield is obtained from the  $M_{bc}$  distribution (Fig. 2). In Fig. 3 we show that the ratio between the number of events in the sideband and the signal regions of the SFW variable is independent of the beam constrained

mass  $M_{bc}$  according to a MC calculation assuming continuum  $q\bar{q}$  production. This observation is consistent with the background estimated using the off-resonance data. Thus, the SFW sideband data can be used to model the background shape of the  $M_{bc}$  spectrum in the absence of a substantial sample of off-resonance data. We fit the  $M_{bc}$  distribution with a background shape taken from the SFW sideband data and a signal shape obtained from MC simulation.

We observe 222 events in the signal region  $M_{bc} > 5.27 \text{ GeV}/c^2$ , of which  $115.5 \pm 7.7$  is the estimated background contribution, and is consistent with the MC expectation. An excess of  $106.5 \pm 16.8$  events is clearly seen at the  $B$  meson mass with a mass resolution of  $4.4 \text{ MeV}/c^2$  and a signal-to-background ratio of 0.9.

To correct the recoil mass spectrum  $M_{X_s}$  of Fig. 4 for background, we adopt a different method because the ratio between the number of SFW sideband events and signal events has a finite slope as a function of  $M_{X_s}$  which would introduce an additional systematic error [8]. Instead we use the shape of the  $M_{X_s}$  spectrum determined from MC, whose contribution is normalized to the estimated background of the  $M_{bc}$  distribution. Here we use the SFW sideband sample for a crosscheck only and obtain consistent results for the  $M_{X_s}$  spectrum and the  $B \rightarrow X_s \gamma$  branching fraction.

The signal MC sample is generated as a mixture of the exclusive  $B \rightarrow K^*(892)\gamma$  mode and an inclusive  $B \rightarrow X_s \gamma$  contribution for  $M_{X_s} > 1.15 \text{ GeV}/c^2$  in order to separate the  $K^*(892)$  signal from higher resonances starting with  $K_1(1270)$ . The recoil system  $X_s$  is modelled as an equal mixture of  $\bar{s}d$  and  $\bar{s}u$  states [6]. To simulate the inclusive  $M_{X_s}$  spectrum, we adopt the model by Kagan and Neubert [9] with the  $b$  quark mass parameter  $m_b = 4.75 \text{ GeV}/c^2$ .

In order to determine the fraction of  $K^*(892)\gamma$  decays in the  $B \rightarrow X_s \gamma$  transition,  $r_{K^*\gamma}$ , the migration effects on the reconstructed  $M_{X_s}$  due to misassignment of the  $X_s$  final state have to be considered. The  $M_{X_s}$  spectrum is divided into two regions: the  $K^*(892)$  region below  $1.15 \text{ GeV}/c^2$  and the continuum region between  $1.15 \text{ GeV}/c^2$  and  $2.05 \text{ GeV}/c^2$ . We analyze each of the exclusive and inclusive MC samples, and determine the correction factors to unfold the migration effects in  $r_{K^*\gamma}$ . The  $M_{bc}$  fitting procedure is then iterated using a MC sample with the corrected  $r_{K^*\gamma}$ . It results in  $r_{K^*\gamma} = (11.3 \pm 3.5)\%$ . We note that due to a non-negligible amount of migration between the regions below and above  $2.05 \text{ GeV}/c^2$ , this boundary does not correspond to a sharp value in  $M_{X_s}$  or  $E_\gamma$ . The model calculation with  $m_b = 4.75 \text{ GeV}/c^2$  suggests that 77% of the events reconstructed below  $2.05 \text{ GeV}/c^2$  are genuine and 23% are from the region above  $2.05 \text{ GeV}/c^2$ .

According to the authors of ref. [9], the  $K^*(892)$  contribution can be ap-

proximated by integrating the  $M_{X_s}$  spectrum up to a threshold mass above the  $K^*(892)$  mass, though their model does not explicitly take resonance contributions into account. This integral is sensitive to the parameter  $m_b$ . To match the measured  $K^*(892)$  fraction we varied  $m_b$  and the threshold mass and observed that  $m_b \geq 4.9 \text{ GeV}/c^2$  is disfavored. Therefore we assume  $m_b = (4.75 \pm 0.10) \text{ GeV}/c^2$  as the parameter region to test the model dependence of the branching fraction measurement [10]. Other theoretical input parameters have little impact on the shape of the  $M_{X_s}$  spectrum.

The event selection efficiency is determined from a MC sample that is calibrated with high statistics control data samples for all final state particles. The reconstruction efficiency for the primary photon is obtained using photons with energies between 2 and 3 GeV from the processes  $e^+e^- \rightarrow e^+e^-\gamma$  and  $\eta \rightarrow \gamma\gamma$ . The charged tracking efficiency for momenta relevant to this analysis is obtained by comparing the high momentum  $\eta$  yields for the  $\eta \rightarrow \pi^+\pi^-\pi^0$  and  $\eta \rightarrow \gamma\gamma$  decay modes. The kaon selection efficiency is determined from a sample of  $\phi \rightarrow K^+K^-$  and  $D_s \rightarrow \phi\pi$  decays. The pion rejection efficiency is also determined from the  $\eta \rightarrow \pi^+\pi^-\pi^0$  sample. The  $K_S^0$  and  $\pi^0$  efficiencies are tested with a sample of  $K^*(892)$  decays into  $K^+\pi^-$ ,  $K^+\pi^0$ ,  $K_S^0\pi^+$  and  $K_S^0\pi^0$ . Combining all 16 different channels, the selection efficiency becomes 12.8%. The  $M_{X_s}$ , SFW and  $M_{bc}$  cuts reduce the efficiency by 57%, 50% and 70%, respectively. The SFW cut and the  $\pi^0/\eta$  veto efficiencies are measured with a sample of exclusively reconstructed  $B^- \rightarrow D^0\pi^-$ ,  $D^0 \rightarrow K^-\pi^+$  decays. The final event reconstruction efficiency is 2.58%.

The total systematic error is quoted as a quadratic sum of the systematic errors on the efficiency, the best candidate selection, signal MC statistics, SFW sideband uniformity and the number of  $B\bar{B}$  events. The sensitivity of the cuts to the experimental error on the beam constrained mass  $M_{bc}$  is tested by changing the MC resolution function, and the effect is found to be negligible. The efficiency errors on the 16 different final states are calculated individually and are then combined. The best candidate selection is tested with a  $B^- \rightarrow D^0\pi^-$  sample, which is analyzed using the inclusive reconstruction method of this analysis. The effect of the SFW sideband uniformity is tested by adding a slope to the background distribution within the tolerance level of Fig. 3. The contributions to the systematic error on the branching fraction are given in Table 1.

The fitted signal yield is extrapolated over the entire  $M_{X_s}$  region using the model of ref. [9] with  $m_b = 4.75 \text{ GeV}/c^2$  and corrected for the final states that are not reconstructed. The analysis is repeated for  $m_b = 4.65 \text{ GeV}/c^2$  and  $4.85 \text{ GeV}/c^2$  to test the model uncertainty. The signal efficiency is found to be 15% lower and 16% higher, respectively. This error and the error on the exclusive to inclusive fraction of typically 5.0% are combined into the theoretical model error.

Finally, we obtain the branching fraction of  $B \rightarrow X_s \gamma$ ,

$$Br(B \rightarrow X_s \gamma) = (3.36 \pm 0.53(\text{stat}) \pm 0.42(\text{sys})^{+0.50}_{-0.54}(\text{th})) \times 10^{-4}$$

where the first error is statistical, the second is systematic and the third is the theoretical model error. Using the central values of the measured  $B \rightarrow X_s \gamma$  branching fraction and the fraction of the  $K^*(892)\gamma$ , we find  $B \rightarrow K^*(892)\gamma$  branching fraction is  $3.8 \times 10^{-5}$ , which is consistent with the  $B \rightarrow K^*(892)\gamma$  branching fraction measurements from CLEO [11] and a separate Belle analysis [12]. In Fig. 5 we show the measured photon spectrum which is corrected for background and for  $M_{X_s}$  cuts by using MC input. This spectrum may be compared with model calculations.

To summarize, we have measured the inclusive branching fraction of  $B \rightarrow X_s \gamma$  decay with the Belle detector. The result is consistent with the SM prediction of  $Br(B \rightarrow X_s \gamma) = (3.28 \pm 0.33) \times 10^{-4}$  [1]. The result is also consistent with previous measurements by the CLEO [13] and ALEPH [14] experiments.

We gratefully acknowledge the efforts of the KEKB group in providing us with excellent luminosity and running conditions and the help with our computing and network systems provided by members of the KEK computing research center. We wish to thank M. Neubert and A. Ali for helpful suggestions on the modelling of the  $B \rightarrow X_s \gamma$  MC. We thank the staffs of KEK and collaborating institutions for their contributions to this work, and acknowledge support from the Ministry of Education, Science, Sports and Culture of Japan and the Japan Society for the Promotion of Science; the Australian Research Council and the Australian Department of Industry, Science and Resources; the Department of Science and Technology of India; the BK21 program of the Ministry of Education of Korea and the Basic Science program of the Korea Science and Engineering Foundation; the Polish State Committee for Scientific Research under contract No.2P03B 17017; the Ministry of Science and Technology of Russian Federation; the National Science Council and the Ministry of Education of Taiwan; the Japan-Taiwan Cooperative Program of the Interchange Association; and the U.S. Department of Energy.

## References

- [1] K. Chetyrkin, M. Misiak, M. Münz, Phys. Lett. B 400 (1997) 206; Erratum ibid. B 425 (1998) 414.
- [2] For example, F. Borzumati, C. Greub, Phys. Rev. D 58 (1998) 074004; M. Ciuchini, G. Degrassi, P. Gambino, G. F. Giudice, Nucl. Phys. B 534 (1998) 3; C. Bobeth, M. Misiak, J. Urban, Nucl. Phys. B 567 (2000) 153.

- [3] KEK accelerator group, KEKB B-Factory Design Report, KEK Report 95-7 (1995), unpublished.
- [4] Belle Collaboration, K. Abe et al., The Belle Detector, KEK Progress Report 2000-4 (2000), to be published in Nucl. Instr. Meth. A.
- [5] R. Brun et al., GEANT 3.21, CERN Report No. DD/EE/84-1 (1987).
- [6] We use the QQ  $B$  meson decay event generator developed by the CLEO collaboration (<http://www.lns.cornell.edu/public/CLEO/soft/QQ>), and the JETSET program, T. Sjöstrand, “PYTHIA 5.6 and JETSET 7.3: Physics and manual,” CERN-TH-6488-92, to hadronize  $q\bar{q}$  and  $X_s$  final states.
- [7] G. Fox and S. Wolfram, Phys. Rev. Lett. 41 (1978) 1581.
- [8] Y. Ushiroda, PhD Thesis, Kyoto University (2001), unpublished, see <http://belle.kek.jp/bdocs/theses.html>.
- [9] A. L. Kagan, M. Neubert, Eur. Phys. J. C 7 (1999) 5.
- [10] The  $m_b$  parameter range is decided on the basis of a private communication with A. Ali.
- [11] CLEO Collaboration, T. Coan et al., Phys. Rev. Lett. 84 (2000) 5283.
- [12] M. Nakao (Belle Collaboration), Studies of Radiative  $B$  Meson Decays with Belle, Proceedings of the 30th International Conference on High Energy Physics, July 2000, Osaka.
- [13] CLEO Collaboration, M. Alam et al., Phys. Rev. Lett. 74 (1995) 2885.
- [14] ALEPH Collaboration, R. Barate et al., Phys. Lett. B 429 (1998) 169.

Table 1

The contributions to the systematic error on the branching fraction.

Photon reconstruction	$\pm 5.3\%$
Charged track reconstruction	$\pm 4.7\%$
Charged kaon selection	$\pm 1.8\%$
Charged pion selection	$\pm 1.1\%$
$K_S^0$ reconstruction	$\pm 1.2\%$
$\pi^0$ reconstruction	$\pm 3.1\%$
SFW efficiency and $\pi^0/\eta$ veto	$\pm 6.8\%$
Best candidate selection	$\pm 2.4\%$
SFW sideband uniformity	$\pm 4.7\%$
Signal MC statistics	$\pm 3.0\%$
Number of $B\bar{B}$ events	$\pm 2.3\%$
Total systematic error	$\pm 12.4\%$

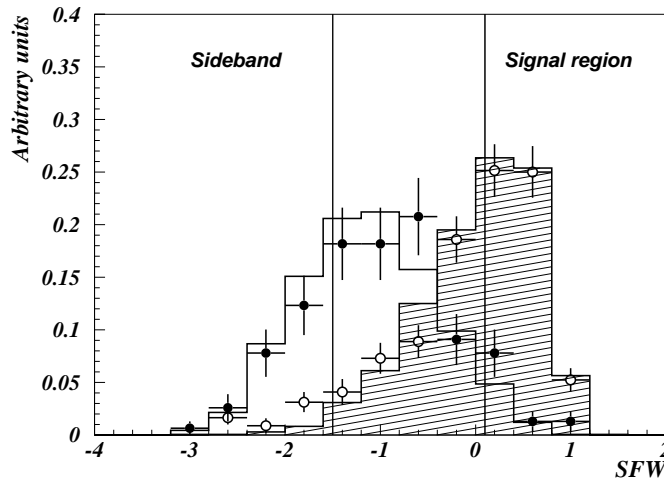


Fig. 1. The distribution of the SFW variable described in the text. The off-resonance background data (solid circles) and the  $q\bar{q}$  MC expectation (open histogram) are compared with the signal distribution of  $B\rightarrow D\pi$  data (open circles) and signal MC (hatched histogram).

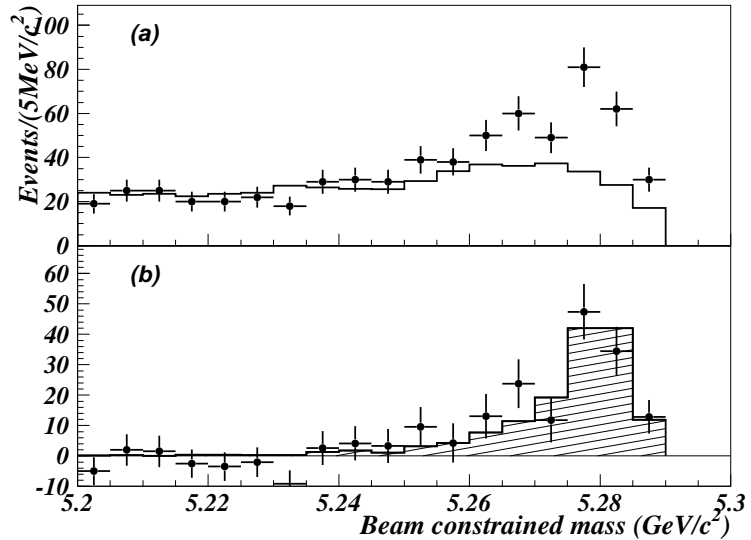


Fig. 2. The beam constrained mass ( $M_B$ ) distribution (a) compared with the total background  $q\bar{q}$  and  $b \rightarrow c$  (open histogram); (b) after background subtraction compared with the signal MC expectation (hatched histogram).

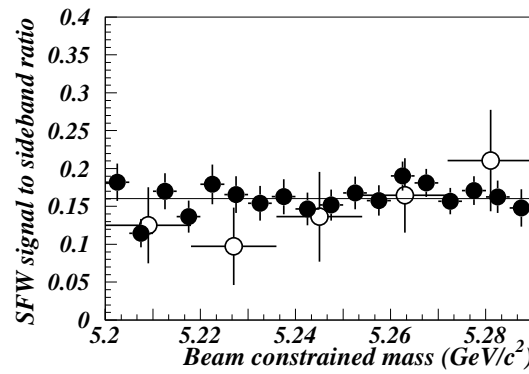


Fig. 3. The ratio of the background events in the SFW signal region to the sideband region as a function of  $M_B$  from the  $q\bar{q}$  MC (solid circles) and off-resonance data (open circles).

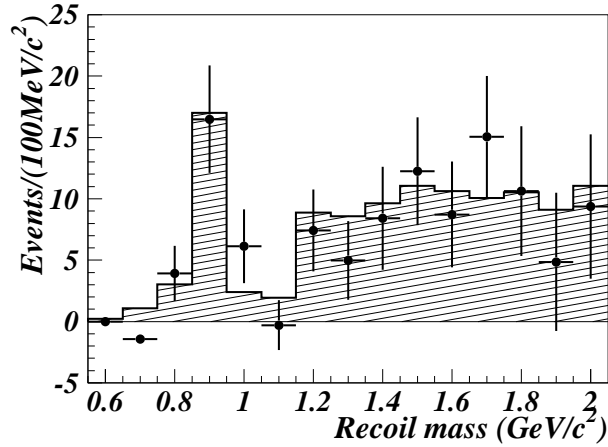


Fig. 4. The recoil mass ( $M_{X_s}$ ) distribution after background subtraction compared with the signal MC expectation (hatched histogram).

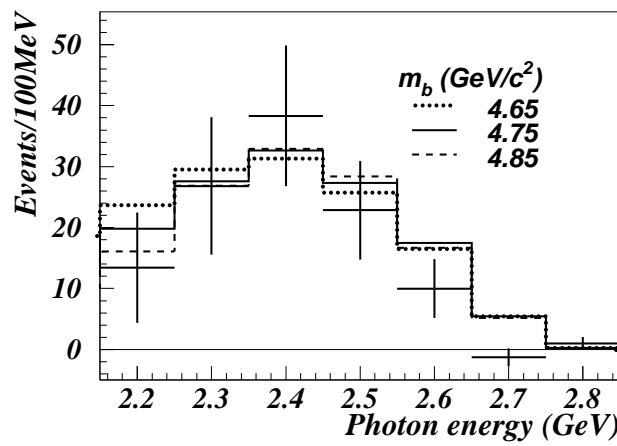


Fig. 5. The photon energy spectrum, background subtracted and corrected for the  $M_{X_s}$  cut-off. The data points are compared with signal MC expectations for three different  $m_b$  parameters.